

# Theoretical investigation of transition data of astrophysical importance in neutral sulphur

W. Li<sup>1</sup>, A. M. Amarsi<sup>2</sup>, and P. Jönsson<sup>3</sup>

<sup>1</sup>State Key Laboratory of Solar Activity and Space Weather, National Astronomical Observatories, Chinese Academy of Sciences

<sup>2</sup>Theoretical Astrophysics, Department of Physics and Astronomy, Uppsala University, Box 516, SE-751 20 Uppsala, Sweden

<sup>3</sup>Department of Materials Science and Applied Mathematics, Malmö University, SE-205 06 Malmö, Sweden

Received 2 September 2025 / Accepted 26 January 2026

## ABSTRACT

Accurate and comprehensive atomic data are essential for the modelling of stellar spectra. Uncertainties in the oscillator strengths of specific lines used for abundance analyses directly translate into uncertainties in the derived elemental abundances; incomplete or biased atomic data sets can impart significant errors in non-local thermodynamic equilibrium (non-LTE) modelling. Theoretical calculations of atomic data are therefore crucial to supplement the limited experimental results. In this work, we present extensive atomic data, including oscillator strengths, transition rates, and lifetimes for 1,730 electric-dipole (E1) transitions among 107 levels in neutral sulphur ( $S\,\text{i}$ ) using the multi-configuration Dirac–Hartree–Fock (MCDHF) and relativistic-configuration-interaction (RCI) methods. These levels belong to the configurations  $3p^3\text{np}$  ( $n = 3 - 7$ ),  $3p^3\text{nf}$  ( $n = 4, 5$ ),  $3s3p^5$ ,  $3p^3\text{ns}$  ( $n = 4 - 7$ ), and  $3p^3\text{nd}$  ( $n = 3 - 6$ ). The accuracy of the computed transition rates is assessed by combining the comparison of the differences in transition rates between the Babushkin and Coulomb gauges with a cancellation-factor (CF) analysis. Approximately 16% of the ab initio results achieved an accuracy classification of A-B, corresponding to uncertainties within 10%, as defined by the Atomic Spectra Database of the National Institute of Standards and Technology (NIST ASD). Applying a fine-tuning technique was found to significantly improve the accuracy of the results in the Coulomb gauge, thereby improving the consistency between the Babushkin and Coulomb gauges; about 24% of the fine-tuned transition data are assigned to the accuracy classes A-B.

**Key words.** Atomic data — Atomic processes — Methods: numerical — Sun: abundances — Stars: abundances

## 1. Introduction

Spectroscopy is a powerful tool in astrophysics, providing critical insights into the physical conditions and chemical abundances of stars (Tennyson 2019). Sulphur, as one of the most abundant elements in the Universe, exhibits a wealth of spectral features across multiple wavelength bands that have been observed with both space- and ground-based facilities (e.g. Durrance et al. 1983; Skillman & Kennicutt 1993; Carpenter et al. 1994). These lines serve as powerful diagnostics for probing stellar atmospheres, the interstellar medium, and galaxies (e.g. Judge 1988; Feaga et al. 2002; Anderson et al. 2013). In particular, as an  $\alpha$  element, sulphur is routinely employed in the study of Galactic chemical evolution (e.g. Nissen et al. 2007; Skúladóttir et al. 2015; Duffau et al. 2017; Costa Silva et al. 2020; da Silva et al. 2023).

Given this importance, it is of interest to reliably infer sulphur abundances in stars and in other astronomical objects. However, accurate analyses of observed sulphur spectra require accurate and complete atomic data sets. Errors in transition data of small sets of diagnostic lines directly impact inferred sulphur abundances; while incomplete or systematically biased atomic data sets could impact the statistical equilibrium in non-local thermodynamic equilibrium (non-LTE) models (e.g. Kamp et al. 2001; Daflon et al. 2003; Takeda et al. 2005; Korotin & Kiselev 2024). Considerable effort has therefore been devoted to both theoretical calculations and laboratory measurements of transition data for neutral sulphur.

On the experimental side, earlier measurements of oscillator strength and transition probabilities between multiplet transitions were reported by Savage & Lawrence (1966), Bridges & Wiese (1967), and Müller (1968). Doering (1990) measured relative oscillator strengths for the  $3p^4\,{}^3P - 3p^3\,{}^4S\,4s\,{}^3S^o$  (1814 Å),  $3p^4\,{}^3P - 3p^3\,{}^2D\,4s\,{}^3D^o$  (1479 Å), and  $3p^4\,{}^3P - 3p^3\,{}^4S\,3d\,{}^3D^o$  (1429 Å) multiplets using the method of electron energy-loss spectroscopy. Delalic et al. (1990) determined the radiative lifetimes of eight different multiplets in the visible range using the high-frequency deflection technique. Beideck et al. (1994) derived oscillator strengths for eight transitions of the multiplets between  $3p^3\,{}^4S\,4s\,{}^3S^o$ ,  $3p^3\,{}^2P\,4s\,{}^3P^o$ , and  $3p^4\,{}^3P$  based on measured mean lifetimes and branching ratios using beam-foil spectroscopic techniques at the Toledo Heavy Ion Accelerator. Based on the oscillator strength reported by Doering (1990) and Beideck et al. (1994), Federman & Cardelli (1995) analysed interstellar spectra towards  $\zeta$ -Oph acquired with the Goddard High-Resolution Spectrograph and obtained a self-consistent set of oscillator strengths for approximately a dozen  $S\,\text{i}$  lines from a curve of growth. More recently, using time-resolved vacuum-ultraviolet laser spectroscopy, Zerne et al. (1997) determined oscillator strengths for the  $3p^3\,{}^4S\,4s\,{}^3S^o_1 - 3p^3\,{}^4S\,4p\,{}^3P_{0,1,2}$  triplet at 10450 Å and Berzinsh et al. (1997) reported lifetimes for twelve states. These lifetime data were combined by Biémont et al. (1998) with their theoretical branching ratios from relativistic Hartree–Fock (HFR) calculations to deduce a consistent set of oscillator strengths for vacuum ultraviolet lines.

Besides experimental measurements, there are also a number of theoretical calculations of the transition data for S I. [Ganas \(1982\)](#) calculated the optical oscillator strengths for the sulphur isoelectric sequence using an analytic atomic independent-particle-model potential. [Kurucz & Peytremann \(1975\)](#) calculated the oscillator strength semi-empirically using scaled Thomas-Fermi-Dirac radial wave functions and eigenvectors found through least-squares fits to observed energy levels. [Ho & Henry \(1985\)](#), [Fleming & Hibbert \(1999\)](#), [Tayal \(1998\)](#), and [Chen & Msezane \(1997\)](#) did the calculations using the CIV3 code based on configuration-interaction (CI) method ([Hibbert 1975](#)). [Fawcett \(1986\)](#) calculated the oscillator strengths for allowed  $n=3 - 3$  and  $3 - 4$  transitions of S I with the HFR program package. [Fischer \(1987\)](#) carried out multi-configuration Hartree-Fock (MCHF) calculations for a number of  $3p^3(^2D)nd$   $^3P^0$  terms in S I. More recently, [Froese Fischer et al. \(2006\)](#) reported both allowed electric-dipole (E1) and some forbidden transitions among levels up to  $3p^3(^4S)3d$   $^3D^0$  by including relativistic effects through the Breit-Pauli Hamiltonian. [Zatsarinsky & Bartschat \(2006\)](#), hereafter ZB2006 reported fine structure energies for configurations  $3p^3nl$  of certain levels up to  $n=12$  and the associated E1 oscillator strengths among them using a B-spline box-based multi-channel method. In this calculation, they included CI effects by using a fairly large B-spline basis set and relativistic effects through the Breit-Pauli Hamiltonian. [Deb & Hibbert \(2006\)](#) and [Deb & Hibbert \(2008\)](#), hereafter DH2008 presented oscillator strengths and radiative rates for 2173 E1 transitions among 120 levels using the CIV3 program with a fine-tuning technique. However, as reported by ZB2006, comparisons of oscillator strengths and transition probabilities among various calculations sometimes show large disagreement. The large disagreement between different calculations indicates large uncertainties in the theoretical atomic data, which may have a significant impact on astrophysical spectroscopic analyses. This may be due to the insufficient configuration interactions included in many of the calculations. The most recent work by DH2008 included 300,000 configuration state functions (CSFs) in their CI calculation, which, to our knowledge, is the largest scale calculation for S I to date. However, larger scale calculations, such as those with millions of CSFs, had not been performed until now.

The purpose of this study is to present the results of our extensive calculations using the fully relativistic multi-configuration Dirac–Hartree–Fock (MCDHF) and relativistic configuration interaction (RCI) methods. Here we provide two sets of calculation results. One set was obtained directly from the MCDHF and RCI calculations, which we refer to as the ab initio results. The other set involves fine-tuning of eigenvalues in the RCI calculations, which we refer to as the fine-tuned results. We compare the fine-tuned data with the ab initio results to investigate the effects of fine-tuning on radiative data and lifetimes. The new atomic data set may help with assessing the accuracy of various atomic data via comparisons with other data sets.

This paper is structured into four sections, including the Introduction. Section 2 introduces the theoretical methods and computational schemes. Section 3 presents the results and discussions on energy levels, transition data, and lifetimes. Section 4 includes our conclusion.

## 2. Method

### 2.1. Multi-configuration Dirac–Hartree–Fock approach

The calculations were performed using the MCDHF and RCI methods, based on a Dirac–Coulomb Hamiltonian, which are

implemented in the general-purpose relativistic atomic-structure package GRASP2018<sup>1</sup>. We briefly outline the methods in this section and refer the reader to [Grant \(2007\)](#), [Froese Fischer et al. \(2016\)](#), [Froese Fischer et al. \(2019\)](#), and [Jönsson et al. \(2023b\)](#) for details of the MCDHF method and [Jönsson et al. \(2023a\)](#) for a step-by-step instruction manual of the package.

In the MCDHF method, the atomic state wave functions (ASFs,  $\Psi(\gamma^{(j)} PJM)$ ) are expanded over a linear combination of configuration state functions (CSFs,  $\Phi(\gamma_i PJM)$ ):

$$\Psi(\gamma^{(j)} PJM) = \sum_i^{N_{\text{CSFs}}} c_i^{(j)} \Phi(\gamma_i PJM). \quad (1)$$

The CSFs are  $jj$ -coupled multi-electron functions built from products of one-electron Dirac orbitals. The radial parts of the one-electron orbitals and the expansion coefficients of the CSFs are obtained in a relativistic self-consistent field procedure by solving the Dirac–Hartree–Fock radial equations and the configuration interaction eigenvalue problem. The angular integrations needed for the construction of the energy functional are based on the second quantisation method in the coupled tensorial form ([Gaigalas et al. 1997, 2001](#)). Once the radial components of the one-electron orbitals are determined, in the following RCI calculations, higher order interactions, such as the Breit interaction and quantum electrodynamic effects (self-energy and vacuum polarization), are added to the Dirac–Coulomb Hamiltonian. Keeping the radial components fixed, the expansion coefficients of the CSFs for the target states are obtained by solving the configuration interaction eigenvalue problem.

Once the ASFs have been determined from RCI calculations, the radiative E1 transition data (e.g. transition rates  $A$  and weighted oscillator strengths  $\log(gf)$ ) between two states,  $\gamma' P' J'$  and  $\gamma PJ$ , can be computed in terms of reduced matrix elements of the transition operator by summing up reduced matrix elements between all the CSFs for the lower and upper states:

$$\langle \Psi(\gamma PJ) \parallel \mathbf{T}^{(1)} \parallel \Psi(\gamma' P' J') \rangle = \sum_{j,k} c_j c'_k \langle \Phi(\gamma_j PJ) \parallel \mathbf{T}^{(1)} \parallel \Phi(\gamma'_k P' J') \rangle. \quad (2)$$

The transition operator can be expressed in the Babushkin and Coulomb gauges, which in the non-relativistic limit, respectively, correspond to the length and velocity forms. In the limit of including CSFs obtained by all possible excitations to a complete set of orbitals, we may arrive at the exact wave functions to the Dirac equation; this leads to identical values for the Babushkin and Coulomb transition moments ([Grant 1974](#)). However, when approximate multi-electron wave functions are used in practice, the transition data in the two gauges are often different. The relative difference between the values of these two gauges,  $dT = |A_B - A_C|/\max(A_B, A_C)$ , can be used as one indicator of the accuracy of the wave functions ([Froese Fischer 2009; Ekman et al. 2014](#)). It should be noted that  $dT$  should be used in a statistical manner as done in [Papoulia et al. \(2019\)](#) and [Li et al. \(2023a,b\)](#). We discuss this further in Section 3.2.1.

In the MCDHF relativistic calculations, the ASFs are given in terms of  $jj$ -coupled CSFs. In order to identify the computed states and adapt the labelling conventions followed by the astronomers and experimentalists, the ASFs are transformed from  $jj$ -coupling to a basis of  $LSJ$ -coupled CSFs. In the GRASP2018 package, the transformation from  $jj$ - to  $LSJ$ -coupling is done by the jj2lsj program developed by [Gaigalas et al. \(2003, 2004, 2017\)](#).

<sup>1</sup> GRASP is fully open source and is available on GitHub repository at <https://github.com/compas/grasp> maintained by the CompAS collaboration.

Table 1: Summary of the computational schemes for S I.

Parity	MR-MCDHF	MR-RCI	AS	$N_{\text{CSFs}}$
even	$3s^23p^3np$ ( $n = 3 - 8$ ), $3s^23p^3nf$ ( $n = 4, 5$ ), $3p^6$	$3p^6, 3s^23p^3np$ ( $n = 3 - 8$ ), $3s^23p^3nf$ ( $n = 4, 6$ ), $3s3p^3np7d$ ( $n = 3 - 7$ ), $3sp^3nf7d$ ( $n = 4, 5$ ), $3s^23pnp7d^2$ ( $n = 3, 4$ )	{12s, 12p, 11d, 10f, 9g, 8h}	11 049 420
odd	$3s^23p^3ns$ ( $n = 4 - 7$ ), $3s^23p^3nd$ ( $n = 3 - 7$ ) $3s3p^5, 3p^54s$	$3s3p^5, 3s^23p^3ns$ ( $n = 4 - 8$ ), $3p^54s, 3s^23p^3nd$ ( $n = 3 - 7$ ), $3s3p^3ns7d$ ( $n = 4 - 7$ ), $3sp^3nd7d$ ( $n = 3 - 7$ ), $3p^57d, 3s^23p4s7d^2, 3s3p^4np$ ( $n = 4 - 8$ )	{12s, 12p, 11d, 10f, 9g, 8h}	8 146 099

**Notes.** MR-MCDHF and MR-RCI, respectively, denote the multi-reference sets used in the MCDHF and RCI calculations. AS is the active sets of orbitals.  $N_{\text{CSFs}}$  are the numbers of generated CSFs in the final RCI calculations.

## 2.2. Computational schemes

We targeted the states belonging to the  $\{3p^3np$  ( $n = 3 - 7$ ),  $3p^3nf$  ( $n = 4, 5$ )} even configurations and the  $\{3s3p^5, 3p^3ns$  ( $n = 4 - 7$ ),  $3p^3nd$  ( $n = 3 - 6$ )} odd configurations. To account for higher order configuration–interaction contributions in the wave functions relative to the target configurations, we employed extended multi-reference (MR) configurations in both MCDHF (MR-MCDHF) and RCI (MR-RCI) calculations. These extended MR sets were determined through the `rcsfm` program in GRASP2018 based on the results of a preliminary calculation. The final MR sets adopted in the MCDHF and RCI calculations, the orbital sets, and the total number of CSFs ( $N_{\text{CSFs}}$ ) for even and odd parities are presented in Table 1.

Our calculations were performed in the extended optimal level scheme (Dyall et al. 1989) for the weighted average of the even and odd parity states. The multi-reference single-double (MR-SD) method was employed to obtain CSF expansions, which allows for single and double (SD) substitutions from MR configurations to orbitals within an active set (AS; Olsen et al. 1988; Sturesson et al. 2007; Froese Fischer et al. 2016). The orbitals in the AS are divided into spectroscopic orbitals, which build the configurations in the MR, and correlation orbitals, which are introduced to correct the initially obtained wave functions.  $1s^22s^22p^6$  was always kept as an inactive closed core. In the MCDHF calculations, the 3s orbitals were kept inactive and the CSF expansions were produced by SD substitutions from all the other valence orbitals of the configurations in the MR-MCDHF. The final wave functions of the target states were determined in a subsequent RCI calculation, which included CSF expansions that were formed by allowing SD substitution from the  $n \geq 3$  sub-shells of the MR-MCDHF configurations and single substitution from the  $n \geq 3$  sub-shells of the additional configurations in the MR-RCI to the active sets of orbitals presented in Table 1. Breit interactions were also taken into account in the RCI calculation. The final even and odd state expansions, respectively, contained 11,049,420 and 8,146,099 CSFs, distributed over different  $J$  symmetries (0–5 for even parity and 0–4 for odd parity).

## 2.3. Fine-tuning

In atomic-structure calculations, fine-tuning or adjustment of the diagonal elements of the Hamiltonian matrix based on experimental energies is a powerful semi-empirical technique that can substantially reduce the deviations between theoretical and experimentally observed energy levels. This technique has been implemented in the CIV3 (Hibbert 1975) program based on the CI method and in the ATSP2K (Froese Fischer et al. 2007) pro-

gram based on the MCHF method. It has been successfully applied to the calculations of several atomic systems to obtain accurate energy levels and transition parameters (e.g. Lundberg et al. 2001; Corrégé & Hibbert 2004; Froese Fischer & Tachiev 2004). Both of the above methods are based on  $LSJ$ -coupled configuration state functions, where the off-diagonal matrix elements between different  $LS$ -terms are small. However, applying fine-tuning directly to  $jj$ -coupled calculations is challenging due to the large off-diagonal matrix elements. To address this issue, Li et al. (2023) proposed a method to convert the Hamiltonian from  $jj$ -coupling to one in  $LSJ$ -coupling, where fine-tuning can be applied, and return to the  $jj$ -coupling form. The procedure was successfully implemented in GRASP2018 through two new programs `jj2lsj_2022` and `rfinetune`. They also demonstrated that fine-tuning, using C III and B I as examples, significantly improved the accuracy of transition rates and lifetimes, showing clear improvements compared to ab initio calculations. The  $LS$ -composition analysis of the ab initio results reveals that, with a few exceptions in  $3p^3(^4S)7p\ ^3P$  and  $3s3p^5\ ^3P$  states, most states in S I can be well described with relatively pure  $LSJ$ -coupling. Therefore, we adopted the same approach as that employed in Li et al. (2023).

In this work, we applied our fine-tuning procedure for the even and odd states using the MR-RCI set, based on experimental energies from the Atomic Spectra Database of the National Institute of Standards and Technology (NIST ASD) (Kramida et al. 2024). It should be noted that while we were preparing the paper, NIST ASD updated the energy levels based on the results from Civiš et al. (2024). Upon careful comparison, we found that the corrections on the energy levels were negligible, with most relative differences being of the order of  $10^{-7}$ . The largest correction occurred in the  $3p^3(^4S)7p\ ^5P_3$ , with a relative difference of  $10^{-4}$ . Such small differences will not have significant impacts on our fine-tuning results. Therefore, we retained the fine-tuning results in this work.

## 3. Results and discussions

### 3.1. Energy levels

The energy levels for the 107 lowest states of S I (56 even states and 51 odd states) from both ab initio and fine-tuning calculations are presented in Table A.1, together with the experimental energies from the recent update of the NIST ASD by Civiš et al. (2024). The numbers in the first column of the table, labelled as ‘No.’ are in the order of the energy levels given in the NIST ASD. Figure 1 shows the energy differences between calculated data and NIST ASD values plotted against the excitation energies,

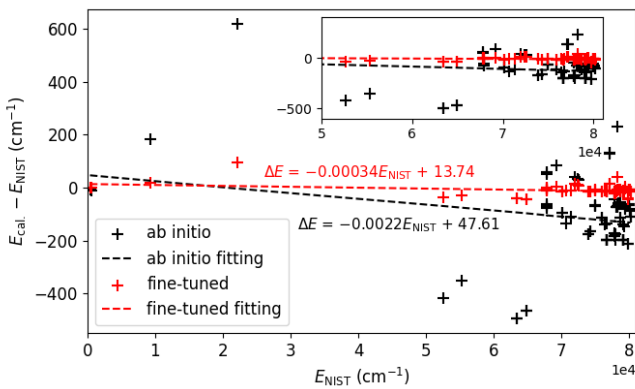


Fig. 1: Energy differences as a function of excitation energies provided by NIST ASD. The dashed black and red lines are the linear fit to the data from ab initio (black plus) and fine-tuning (red plus) calculations, respectively. The inset in the upper right shows an enlarged view for  $E_{\text{NIST}} > 5 \times 10^4 \text{ cm}^{-1}$ .

$E_{\text{NIST}}$ . The agreement between the computational and experimental energies is systematically improved after fine-tuning; the systematic error of computational excitation energies decreases from 0.22% to 0.03%, and the root-mean-square deviation decreases from  $188.5 \text{ cm}^{-1}$  to  $20.3 \text{ cm}^{-1}$ . Especially for the energy levels of  $3p^4 \ ^1S_0$ ,  $3p^3(^4S)4s \ ^5S_0$ ,  $^3S_1$ , and  $3p^3(^4S)4p \ ^5P_{1,2,3}$ ,  $^3P_{0,1,2}$ , the ab initio energies are rather far away (more than  $300 \text{ cm}^{-1}$ ) from the experimental energies; in contrast, the fine-tuned energies are all within  $50 \text{ cm}^{-1}$  of the experimental values, except for  $3p^4 \ ^1S_0$ , which differs by  $96 \text{ cm}^{-1}$ . In addition, fine-tuning can help correct the energy positions of the levels, where the positions refer to the level locations arranged in terms of the excitation energies. For example, in the ab initio calculation, the  $3p^3(^2P)4s \ ^1P_1$  state is higher than the  $3p^3(^2D)4p \ ^3F$  states and in the wrong position compared to experimental data. Fine-tuning brings the energy into the correct position with a corresponding slightly decreased mixing with the  $3p^3(^2D)3d \ ^1P_1$  perturber into the  $3p^3(^2P)4s \ ^1P_1$  state.

Further iterations of fine-tuning could potentially yield results even closer to the experimental energies. Considering the total time cost involved in the fine-tuning process and the recalculation of the wave functions and transition properties, as well as the fact that currently available results have already reached a level of accuracy that is challenging to attain simply by increasing the size of the CSF basis, especially given that the present work involved over ten million CSFs in the calculations, we believe that the current results are sufficient to study the impact of fine-tuning on transition data.

### 3.2. Transition data

The transition parameters computed from both ab initio and fine-tuning calculations for 1,730 E1 transitions among the 107 energy levels given in Table A.1 are presented in Table A.2; the full table is available at the CDS. Note that the wavelengths listed in all tables of the paper are derived from the experimental energy levels in the NIST ASD, which are originally from Civiš et al. (2024); the transition data, including weighted oscillator strengths,  $\log(gf)$  and transition rates,  $A$ , for both ab initio and fine-tuned results are all adjusted using experimental wavelengths.

#### 3.2.1. Accuracy assessment

We evaluated the accuracy of our computed transition data following the method used in Li et al. (2023b). This approach is based on grouping transitions based on the magnitude of  $A$  values. For  $S\ 1$ , we chose six groups such that  $A < 10^{-2} \text{ s}^{-1}$ ,  $10^{-2} \leq A < 10^0 \text{ s}^{-1}$ ,  $10^0 \leq A < 10^3 \text{ s}^{-1}$ ,  $10^3 \leq A < 3.5 \times 10^5 \text{ s}^{-1}$ ,  $3.5 \times 10^5 \leq A < 10^7 \text{ s}^{-1}$ , and  $A \geq 10^7$ . Next, we calculated the averaged  $dT_{\text{av}}$  for each group. As we mentioned in Section 2.1, the gauge difference parameter should only be used as an uncertainty estimate in a statistical manner for a group of transitions with similar properties. As such, we define  $d\tilde{T}$  as  $\max(dT, dT_{\text{av}})$  to replace  $dT$  as the gauge difference indicator for individual transitions. We then folded the cancellation-factor (CF) into the analysis. This is a numerical measure of the cancellation effect in the computation of transition matrix elements (e.g. Cowan 1981; Zhang et al. 2013; Gaigalas et al. 2020). A small CF (generally under about 0.1 or 0.05 as given in Cowan (1981)) indicates a strong cancellation effect, resulting in computed transition parameters with large uncertainties.

The final accuracy class for each computed transition rate was estimated by a combined analysis of the  $d\tilde{T}$  and CF parameters. Based on the above procedure, we divided the accuracy into five classes, following the definition conventions of the accuracy classification in the NIST ASD. The A, B, C, D, and E classes correspond to the {A, A+, and AA}, {B+ and B}, {C+ and C}, {D+ and D}, and E classes, respectively, as defined by the NIST ASD. The definitions of  $d\tilde{T}$  and CF for each accuracy class are as follows:

- A ( $\leq 3\%$ ):  $d\tilde{T} \leq 3 \text{ & } \text{CF} \geq 0.1$
- B ( $\leq 10\%$ ):  $3 < d\tilde{T} \leq 10 \text{ & } \text{CF} \geq 0.1 \text{ or } d\tilde{T} \leq 3 \text{ & } \text{CF} < 0.1$
- C ( $\leq 25\%$ ):  $10 < d\tilde{T} \leq 25 \text{ & } \text{CF} \geq 0.1 \text{ or } 3 < d\tilde{T} \leq 10 \text{ & } \text{CF} < 0.1$
- D ( $\leq 50\%$ ):  $25 < d\tilde{T} \leq 50 \text{ & } \text{CF} \geq 0.1 \text{ or } 10 < d\tilde{T} \leq 25 \text{ & } \text{CF} < 0.1$
- E ( $> 50\%$ ):  $d\tilde{T} > 50 \text{ or } 25 < d\tilde{T} \leq 50 \text{ & } \text{CF} < 0.1$

We provide the estimated accuracy class for each transition in Table A.2; these were defined based on the above procedure for both ab initio and fine-tuned results. We hope that this information can provide data users with a reference for data quality. Taking the Babushkin gauge as an example, the percentage fraction of each accuracy class is as follows:

- ab initio : A: 2.1%; B: 13.8%; C: 30.0%; D: 28.6%; E: 25.5%
- fine-tuned : A: 9.1%; B: 15.1%; C: 26.1%; D: 26.8%; E: 22.9%

The reason for the high proportion of lower accuracy data is that among the 1,730 transition data, approximately 50% are  $LS$ -forbidden inter-combination transitions (IC), including two-electron one-photon (TEOP) transitions involving the  $3s3p^5$  energy levels. These transitions are governed by electron correlation effects, which are difficult to calculate accurately. In high-accuracy classes A and B, over 80% of the transitions are  $LS$ -allowed, whereas in the low-accuracy classes D and E, more than 70% are  $LS$ -forbidden IC transitions.

The statistical results indicate that the proportion of high-accuracy results in classes A and B obtained from the fine-tuned calculations is higher than that from the ab initio calculations. The primary reason for this difference is that fine-tuning reduces the overall differences in the transition data between the Babushkin and Coulomb gauges.

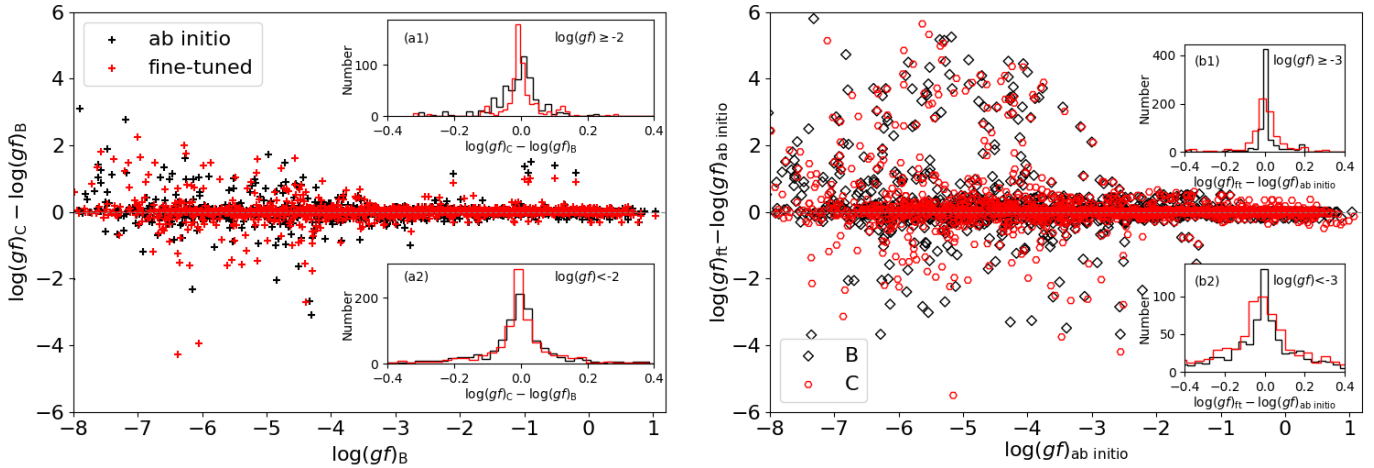


Fig. 2: Left: Comparison of  $\log(gf)$  between Babushkin and Coulomb gauges for ab initio (black plus) and fine-tuned (red plus) results, respectively. Insets (a1) and (a2) show the histograms of the  $\log(gf)$  differences for transitions with  $\log(gf) \geq -2$  and  $\log(gf) < -2$ , respectively. Right: Comparison of  $\log(gf)$  between ab initio and fine-tuned calculations for Babushkin (black diamond) and Coulomb gauges (red hexagon), respectively. Insets (b1) and (b2) show the histograms of the  $\log(gf)$  differences for transitions with  $\log(gf) \geq -3$  and  $\log(gf) < -3$ , respectively.

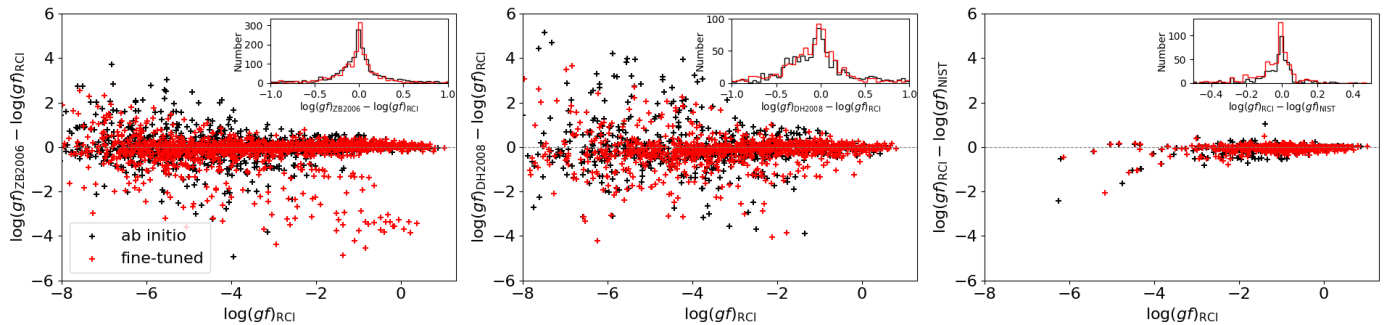


Fig. 3: Comparison of  $\log(gf)$  from the current study with those from previous works. Left: ZB2006 (Zatsarinny & Bartschat 2006). Middle: DH2008 (Deb & Hibbert 2008). Right: NIST ASD (Kramida et al. 2024). The data in NIST ASD were compiled from various sources, including Müller (1968); Beideck et al. (1994); Biémont et al. (1996, 1998); Zerne et al. (1997); Froese Fischer et al. (2006) and Zatsarinny & Bartschat (2006). Babushkin results from present ab initio (black plus) and fine-tuned (red plus) RCI calculations are used in the comparison. The inset figures show the histograms of the distribution of the number of transitions for the differences in  $\log(gf)$ . Note that the y-axis range is consistent across all plots in Figures 2 and 3.

### 3.2.2. Comparison between Babushkin and Coulomb gauges

The left panel of Figure 2 presents the differences in  $\log(gf)$  values between the Babushkin and Coulomb gauges. The histograms (insets (a1) and (a2)) show the distribution of the gauge difference for transitions with  $\log(gf) \geq -2$  and  $\log(gf) < -2$ , respectively. Both the ab initio and fine-tuned data show good agreement between the two gauges, with 73% of the total of 1,730 transitions differing by less than 0.1 dex. For transitions with  $\log(gf)$  greater than -2.0, approximately 86% agree within 0.1 dex between the two gauges for both ab initio and fine-tuned results. In the same subset, as can be seen from the histogram (a1) in the left panel of Figure 2, the number of transitions with differences between the two gauges greater than 0.05 dex is higher for the ab initio results (33%) than for the fine-tuned results (23%). This indicates that fine-tuning can enhance the consistency between the Babushkin and Coulomb gauges to a certain degree, which accounts for the higher proportion of high-accuracy data in the fine-tuned results compared to those obtained from ab initio calculations, as demonstrated in Section 3.2.1.

Generally, stronger transitions show better agreement between the Babushkin and Coulomb gauges. However, we observed six outliers in the range of -1 to 0 of  $\log(gf)_B$  in Figure 2. These are transitions between high Rydberg states  $3p^3(^4S)7p\,^3P_{0,1,2}$  and  $3p^3(^4S)6d\,^3D_{1,2,3}^0$ . Despite the large differences (by 1–1.5 dex) between the Babushkin and Coulomb gauges for these transitions, the ab initio and fine-tuned data in the Babushkin gauge show excellent agreement, with deviations of less than 0.01 dex, while the results in the Coulomb gauge differ by 0.2–0.5 dex. Although all six transitions are classified as E accuracy class based on the method described in Section 3.2.1, we suggest that the Babushkin gauge data may be more reliable for these transitions.

### 3.2.3. Comparison between ab initio and fine-tuned results

The right panel of Figure 2 presents a comparison of  $\log(gf)$  values between the fine-tuned and the ab initio results. The histograms (insets (b1) and (b2)) display the distribution of the differences for transitions with  $\log(gf) \geq -3$  and  $\log(gf) < -3$ , respectively. It is important to note that all data, including wave-

lengths and transition data, were adjusted to match the experimental energy levels, ensuring that the differences shown in the figure are solely due to the changes in mixing coefficients caused by fine-tuning. From this comparison, we observe that fine-tuning has a significant impact on  $\log(gf)$  values, with approximately 42% of the Babushkin data (and 45% of the Coulomb gauge data) showing changes greater than 0.1 dex. Second, as can be seen from the histogram (b1), the effect of fine-tuning is more pronounced on the Coulomb gauge results than on the Babushkin gauge data. For example, among transitions with  $\log(gf)$  greater than  $-3.0$ , 42% of the Coulomb data show changes greater than 0.05 dex, compared to 26% of the Babushkin data. Third, fine-tuning has a more substantial effect on weak transitions than on strong transitions. The histograms show that 44% of transitions with  $\log(gf) < -3$  have a change in the Babushkin gauge greater than 0.2 dex, compared to 9% of transitions with  $\log(gf) \geq -3$ .

Despite ongoing debates concerning the choice of the appropriate gauge (e.g. Starace 1971; Hibbert 1974; Cowan 1981; Papouli et al. 2019; Gaigalas et al. 2024), the Babushkin gauge is generally considered to yield more reliable transition results, as it better describes the outer part of the wave functions that governs the atomic transitions (Hibbert 1974). In addition, the contributions from the negative-energy states were not taken into account in the MCDHF and RCI calculations, which have negligible effects on the Babushkin gauge results but can affect the Coulomb gauge results significantly, especially for the weak IC transitions; this further suggests that the Babushkin gauge results appear to be more reliable (Chen et al. 2001). This explains the findings presented in Figure 2 and the conclusions in Section 3.2.1 and 3.2.2, which namely show that fine-tuning can better improve the less accurate results in the Coulomb gauge, thereby enhancing the agreement between the Babushkin and Coulomb gauges and consequently improving the overall accuracy. Furthermore, the transition matrix element in Coulomb gauge contains a dependence on the transition energy, making it more sensitive to fine-tuning. For these reasons, the greater impact of fine-tuning on the Coulomb gauge than on the Babushkin gauge is expected.

### 3.2.4. Comparison with previous theoretical and experimental results

In Figure 3, our ab initio and fine-tuned  $\log(gf)$  results are compared with the data from ZB2006 (1719 transitions), DH2008 (1001 transitions), and NIST ASD<sup>2</sup> (528 transitions). ZB2006 is based on the B-spline box-based multi-channel method, while DH2008 is based on CI methods with fine-tuning. The histograms in each panel show the statistical distribution of the differences between our results and the others. Overall, our results show better agreement with ZB2006 than with DH2008. For example, among transitions with  $\log(gf)$  greater than  $-3.0$ , 68.4% (66.9%) of the ab initio (fine-tuned) data agree within  $\pm 0.1$  dex with ZB2006, while only 44.6% agree with DH2008.

However, some unexpected large deviations are observed in the lower right corner of the left panel in Figure 3, indicating that fine-tuning leads to large discrepancies of  $>1.0$  dex compared with ZB2006 data for certain transitions. Most of these transitions are IC transitions between  $3p^3(^2D)4p\ ^1P$ ,  $3p^3(^4S)nd$  ( $n = 3, 4, 5, 6$ )  $^3D^o$ ,  $^5D^o$  and

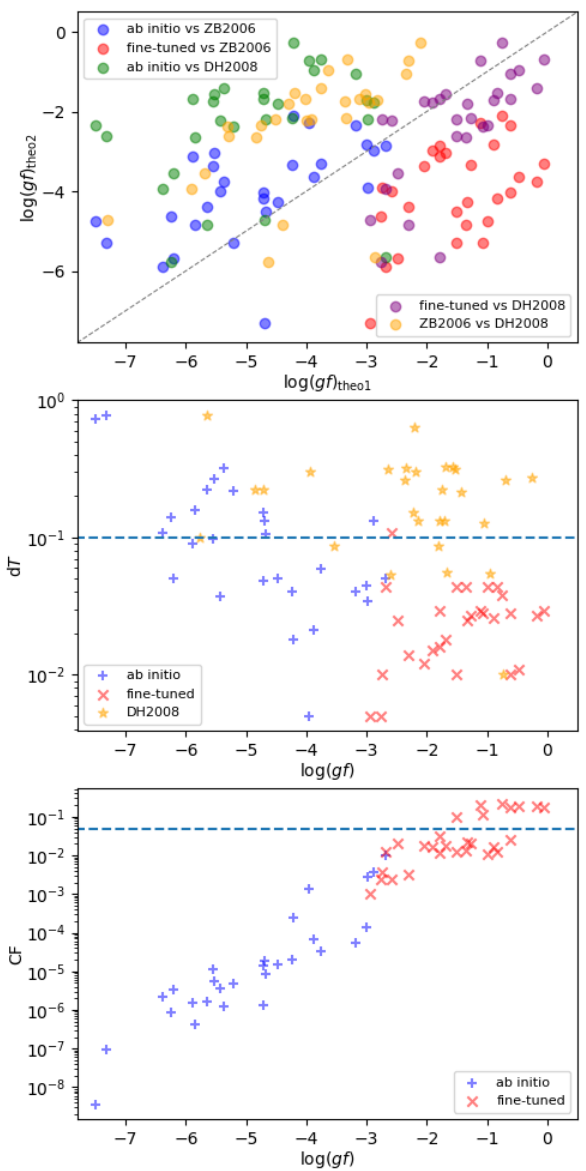


Fig. 4: Upper panel: Comparison of theoretical  $\log(gf)$  values for transitions with  $\log(gf)_{\text{RCI}} > -3.0$  and  $\Delta \log(gf) > 1.0$  dex shown in the left and middle panels of Figure 3. Middle panel: Scatter plot of  $dT$  values. Lower panel: Scatter plot of  $CF$  values. The dashed lines in the middle panel and the lower panel represent  $dT = 0.1$  and  $CF = 0.05$ , respectively. ZB2006: Zatsaranny & Bartschat (2006); DH2008: Deb & Hibbert (2008).

$3p^3(^4S)nf$  ( $n = 3, 4, 5$ )  $^3F$ ,  $^5F$ . IC transitions are directly caused by the mixing of states, and their theoretical transition rates are very sensitive to the quality of the wave functions; the accurate calculation of their transition data is more challenging than for  $LS$ -allowed transitions. In the upper panel of Figure 4, we compare the results of the anomalous transitions for which both ZB2006 and DH2008 data are available. As can be seen from the figure, our fine-tuned data are the largest, while our ab initio data are the smallest among all the calculated results. It is also interesting to note that, despite the considerable differences among various results, our fine-tuned data show better agreement with the fine-tuned results of DH2008, while the ab initio results are closer to ZB2006. Upon closer inspection of the energy levels associated with these ‘anomalous’ transitions, we observe no

<sup>2</sup> Note that some  $\log(gf)$  values for  $S1$  transitions in NIST ASD are anomalous (Alexander Kramida, private communication), while the line strength,  $S$ , and oscillator strength,  $f$ , values are correct. The  $\log(gf)$  values from NIST ASD adopted in this paper were all calculated from the  $f$  values.

Table 2: Comparison of experimental and theoretical weighted oscillator strength,  $\log(gf)$ , for S I.

Upper State	Lower State	$\lambda_{\text{vac.}}$ (Å)	ab initio		Fine-tuned		ZB2006 <sup>a</sup>	DH2008 <sup>b</sup>		Experiments
			B	C	B	C		B	C	
3p <sup>3</sup> ( <sup>2</sup> P)4s 3P <sub>2</sub> <sup>o</sup>	3p <sup>4</sup> ( <sup>3</sup> P) 3P <sub>2</sub>	1295.653	-0.389	-0.397	-0.391	-0.398	-0.385	-0.412	-0.434	-0.362±0.030 <sup>c</sup>
3p <sup>3</sup> ( <sup>2</sup> P)4s 3P <sub>1</sub> <sup>o</sup>	3p <sup>4</sup> ( <sup>3</sup> P) 3P <sub>2</sub>	1296.174	-0.874	-0.882	-0.878	-0.886	-0.870	-0.888	-0.907	-0.959±0.039 <sup>c</sup>
3p <sup>3</sup> ( <sup>2</sup> P)4s 3P <sub>2</sub> <sup>o</sup>	3p <sup>4</sup> ( <sup>3</sup> P) 3P <sub>1</sub>	1302.336	-0.801	-0.809	-0.801	-0.808	-0.805	-0.827	-0.845	-0.815±0.043 <sup>c</sup>
3p <sup>3</sup> ( <sup>2</sup> P)4s 3P <sub>1</sub> <sup>o</sup>	3p <sup>4</sup> ( <sup>3</sup> P) 3P <sub>1</sub>	1302.862	-1.078	-1.087	-1.078	-1.086	-1.074	-1.084	-1.103	-0.932±0.067 <sup>c</sup>
3p <sup>3</sup> ( <sup>2</sup> P)4s 3P <sub>0</sub> <sup>o</sup>	3p <sup>4</sup> ( <sup>3</sup> P) 3P <sub>0</sub>	1305.883	-0.910	-0.919	-0.910	-0.917	-0.914	-0.921	-0.939	-0.824±0.038 <sup>c</sup>
3p <sup>3</sup> ( <sup>4</sup> S)4s 3S <sub>1</sub> <sup>o</sup>	3p <sup>4</sup> ( <sup>3</sup> P) 3P <sub>2</sub>	1807.312	-0.367	-0.374	-0.370	-0.379	-0.371	-0.369	-0.394	-0.319±0.032 <sup>c</sup>
3p <sup>3</sup> ( <sup>4</sup> S)4s 3S <sub>1</sub> <sup>o</sup>	3p <sup>4</sup> ( <sup>3</sup> P) 3P <sub>1</sub>	1820.342	-0.597	-0.605	-0.600	-0.610	-0.601	-0.599	-0.624	-0.593±0.056 <sup>c</sup>
3p <sup>3</sup> ( <sup>4</sup> S)4s 3S <sub>1</sub> <sup>o</sup>	3p <sup>4</sup> ( <sup>3</sup> P) 3P <sub>0</sub>	1826.245	-1.077	-1.084	-1.080	-1.089	-1.080	-1.078	-1.103	-1.252±0.085 <sup>c</sup>
Abundance diagnostic S I lines										
3p <sup>3</sup> ( <sup>4</sup> S)5p 5P <sub>3</sub>	3p <sup>3</sup> ( <sup>4</sup> S)4s 5S <sub>2</sub> <sup>o</sup>	4695.422	-1.667	-1.690	-1.675	-1.686	-1.716	-1.599	-1.607	
3p <sup>3</sup> ( <sup>4</sup> S)5p 5P <sub>2</sub>	3p <sup>3</sup> ( <sup>4</sup> S)4s 5S <sub>2</sub> <sup>o</sup>	4696.753	-1.825	-1.849	-1.833	-1.845	-1.873	-1.753	-1.757	
3p <sup>3</sup> ( <sup>4</sup> S)5d 5D <sub>2</sub> <sup>o</sup>	3p <sup>3</sup> ( <sup>4</sup> S)4p 5P <sub>3</sub>	6758.611	-1.858	-1.896	-1.857	-1.869	-1.784			
3p <sup>3</sup> ( <sup>4</sup> S)5d 5D <sub>3</sub> <sup>o</sup>	3p <sup>3</sup> ( <sup>4</sup> S)4p 5P <sub>3</sub>	6758.886	-1.014	-1.051	-1.012	-1.024	-0.940			
3p <sup>3</sup> ( <sup>4</sup> S)5d 5D <sub>4</sub> <sup>o</sup>	3p <sup>3</sup> ( <sup>4</sup> S)4p 5P <sub>3</sub>	6759.043	-0.428	-0.465	-0.427	-0.438	-0.353			
3p <sup>3</sup> ( <sup>4</sup> S)4d 5D <sub>0</sub> <sup>o</sup>	3p <sup>3</sup> ( <sup>4</sup> S)4p 5P <sub>1</sub>	8672.585	-0.911	-0.962	-0.918	-0.932	-0.908	-0.826	-0.873	
3p <sup>3</sup> ( <sup>4</sup> S)4d 5D <sub>4</sub> <sup>o</sup>	3p <sup>3</sup> ( <sup>4</sup> S)4p 5P <sub>3</sub>	8697.023	+0.047	-0.004	+0.040	+0.027	+0.052	+0.186	+0.182	
3p <sup>3</sup> ( <sup>4</sup> S)4p 3P <sub>2</sub>	3p <sup>3</sup> ( <sup>4</sup> S)4s 3S <sub>1</sub> <sup>o</sup>	10458.308	0.259	+0.273	+0.259	+0.262	+0.256	+0.270	+0.274	+0.250±0.009 <sup>d</sup>
3p <sup>3</sup> ( <sup>4</sup> S)4p 3P <sub>0</sub>	3p <sup>3</sup> ( <sup>4</sup> S)4s 3S <sub>1</sub> <sup>o</sup>	10459.618	-0.440	-0.426	-0.440	-0.436	-0.444	-0.429	-0.426	-0.447±0.011 <sup>d</sup>
3p <sup>3</sup> ( <sup>4</sup> S)4p 3P <sub>1</sub>	3p <sup>3</sup> ( <sup>4</sup> S)4s 3S <sub>1</sub> <sup>o</sup>	10462.267	+0.037	+0.051	+0.037	+0.041	+0.035	+0.048	+0.052	+0.030±0.010 <sup>d</sup>

**Notes.** B: Babushkin gauges. C: Coulomb gauges. The vacuum wavelengths are used in the table.

(<sup>a</sup>) Zatsariny & Bartschat (2006). (<sup>b</sup>) Deb & Hibbert (2008). (<sup>c</sup>) Beam-foil technique by Beideck et al. (1994). (<sup>d</sup>) Laser spectroscopy by Zerne et al. (1997).

tendency for the fine-tuning process to ‘over-correct’ for inaccuracies in energy separations. In the middle and lower panels of Figure 3, we show the distribution of the  $dT$  and CF parameters. It is clear that the fine-tuned results have better consistency between the Babushkin and Coulomb gauges than the ab initio and the DH2008 results. The fine-tuned results exhibit larger CF values than the ab initio data. Based on the accuracy assessment using the  $d\tilde{T}$  & CF method in Section 3.2.1, all transitions from the fine-tuning calculations in Figure 4 have an accuracy class better than C (i.e. A, B or C), while all results from the ab initio calculations are worse than class C (i.e. C, D, or E). Therefore, with regard to a  $dT$  and CF assessment, the fine-tuned results are considered more accurate. We hope for precise experimental measurements in the future to verify them.

Of the 1730 transitions presented in this work, data for 528 of them are available in NIST ASD; they were compiled by Kaufman & Martin (1993) and Podobedova et al. (2009). These data mainly consist of the stronger transitions ( $S \geq 0.01$ ) from ZB2006, while the remaining transitions were sourced from other theoretical calculations (Biémont et al. 1996, 1998; Froese Fischer et al. 2006; Zatsariny & Bartschat 2006) and experimental measurements (Müller 1968; Beideck et al. 1994; Zerne et al. 1997). NIST ASD critically compiled and assessed the uncertainties associated with these results. A comparison of our results with these compiled data helped us assess the reliability of our calculated results. A comparison between our calculated results and the data from NIST ASD is presented in the right panel of Figure 3. We can see that our calculated data, both ab initio and fine-tuned, agree well with the recommended  $\log(gf)$  values from NIST ASD, with approximately 74% of the results falling within  $\pm 0.1$  dex and 54% falling within  $\pm 0.05$  dex.

Specifically, the results for the transitions with available experimental measurements and for the ten transitions used as solar abundance diagnostics are presented in Table 2. The theoretical re-

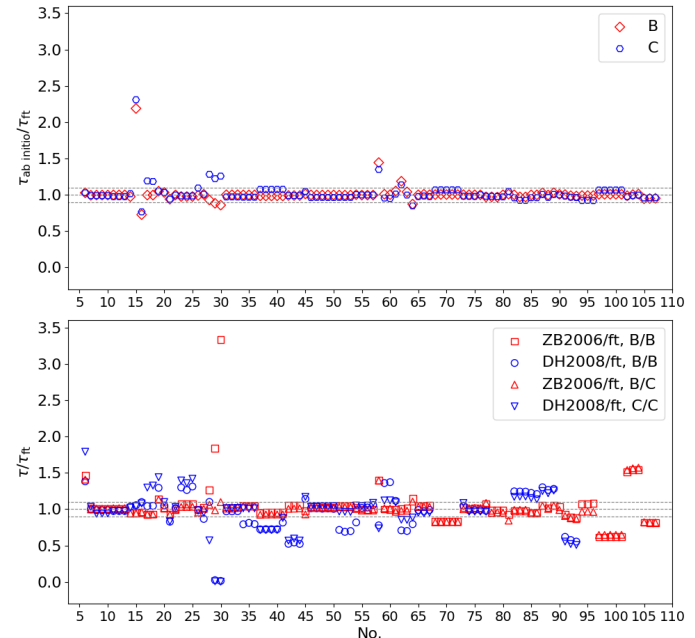


Fig. 5: Upper: Comparison of fine-tuned lifetimes (ft) between Babushkin (B) and Coulomb (C) gauges. Lower: Comparison of fine-tuned lifetimes with other theoretical results. ZB2006: Zatsariny & Bartschat (2006); DH2008: Deb & Hibbert (2008). ZB2006/ft, B/B: the Babushkin gauge of ZB2006 divided by the Babushkin gauge of fine-tuned lifetimes. The three dashed grey lines represent  $\tau/\tau_{\text{ft}} = 0.9, 1.0, \text{ and } 1.1$ , respectively.

sults include ab initio and fine-tuned RCI calculations, B-splines calculation from ZB2006 and CI calculation from DH2008. The laboratory measured results from Beideck et al. (1994) and

Zerne et al. (1997) are listed in the last column. Beideck et al. (1994) derived the oscillator strengths based on measured mean lifetimes and branching ratios using beam-foil spectroscopic techniques. However, all theoretical results for spectral lines, including 1296.17 Å, 1203.86 Å, 1305.88 Å, 1807.31 Å, and 1826.24 Å, fall outside the experimental uncertainties by Beideck et al. (1994), while different theoretical calculations agree very well with each other to  $\pm 0.03$  dex. We further examined the measured results reported by Müller (1968), which provided the oscillator strengths for individual lines of the 1814 Å and 1299 Å multiplets. As shown in Beideck et al. (1994), the discrepancies between the results of the two experiments are particularly large, with a minimum difference of 0.1 dex in  $\log(gf)$ . This indicates that there may still be considerable uncertainties in the measured results.

The comparison results for the ten visible and near-infrared spectral lines used by Scott et al. (2015) for the abundance analysis of the Sun are shown in the lower half of Table 2. For the 10450 Å triplet lines, different theoretical results and laboratory measurements based on laser spectroscopy by Zerne et al. (1997) agree very well within 0.02 dex, although the results from DH2008 are slightly outside the measurement uncertainties. For all ten transitions, the results from DH2008 are generally larger than those from ZB2006 and present calculations, while our ab initio and fine-tuned results are in overall good agreement with ZB2006. However, for the two 4690 Å lines and the 6750 Å triplet, the differences between our results and those of ZB2006 are large, with the maximum difference reaching 0.07 dex. These lines were used as diagnostics for the solar sulphur abundance (e.g. Caffau et al. 2007; Scott et al. 2015). However, owing to this significant discrepancy, 6750 Å was given zero weight in the recent analysis of Amarsi et al. (2025), and requires for further improvements to the theoretical calculations. Precise laboratory measurements of the oscillator strengths for these diagnostic lines are highly desirable for the future, not only to better constrain theoretical calculations, but also for astrophysical applications. Astrophysical consistency tests may also help to assess the reliability and quality of theoretical data (e.g. Laverick et al. 2019; Korotin & Kiselev 2024), especially when laboratory measurements are unavailable.

### 3.3. Lifetimes

Comparing the calculated lifetimes with the precise measured values can also help to evaluate the overall accuracy of the calculated transition data. Figure 5 presents a comparison of our fine-tuned and ab initio lifetimes in Babushkin and Coulomb gauges, respectively (upper panel), as well as with the results from ZB2006 and DH2008 (lower panel). The ab initio and fine-tuned lifetimes agree very well with each other, except for the levels with #19, #20, #28, #29, #30, and #58 in Table A.1. These levels also exhibit significant discrepancies with the results from ZB2006 and DH2008. For levels with #19, #20, and #58, the large discrepancies between ab initio and fine-tuned lifetimes are due to changes in the mixing coefficients of the CSFs caused by fine-tuning. For example, a level with #58 of  $3p^3(^4S)6p\ ^5P_1$  has a percentage purity of 92% in the ab initio calculation, which is close to pure  $LSJ$ -coupling. In contrast, fine-tuning reduced the percentage purity to 84%, with increased mixing with  $3p^3(^2D)4p\ ^1P_1$  to 7%, which shortens the lifetime of  $3p^3(^4S)6p\ ^5P_1$ . The lifetimes of the triplet states  $3s3p\ ^5\ ^3P_{2,1,0}$  (levels with #28, #29, and #30) are partly determined by the TEOP transitions  $3s3p\ ^5\ ^3P^o - 3s^23p^34p\ ^3P, ^5P$  and the IC transitions  $3s3p\ ^5\ ^3P^o - 3s^23p^4\ ^1D, ^1S$ ; these transitions are driven by electron correlation and are very challenging to compute accurately. The triplet states are found to be strongly

mixed with  $3p^3(^2D)nd\ ^3P^o(n = 3 - 7)$ . For these levels, the lifetimes in the Babushkin gauge are more stable, while fine-tuning causes larger changes in the Coulomb gauge. This is consistent with the results discussed in Section 3.2.3, which namely show that fine-tuning has a greater impact on the transition data in the Coulomb gauge.

Overall, the comparison in the lower panel of Figure 5 shows that our results have better agreement with those from ZB2006 than with DH2008. Among the 78 levels with three sets (ZB2006, DH2008 and our calculation) of lifetimes available, 69 of them show agreement with the results from ZB2006 within the range of  $0.9 \leq \tau/\tau_{ft} \leq 1.1$ , while only 35 levels from DH2008 meet this criterion. We also note that our computed lifetimes of the Rydberg states  $3p^3(^4S)6d\ ^5D^o$  (levels with No. #97-#101) quintet and the  $3p^3(^4S)7p\ ^3P$  (levels with No. #102-#104) triplet also show significant differences from those of ZB2006. These levels also experience strong level mixing, especially the  $3p^3(^4S)7p\ ^3P$  triplet, which has a percentage purity of only about 50%. For  $3p^3(^4S)6d\ ^5D_4^o$ , our results, i.e. 266.27/269.21 ns from the ab initio calculation and 264.35/251.99 ns from the fine-tuned calculation, are in very good agreement with the experimental value of  $260 \pm 20$  ns, which was obtained by Delalic et al. (1990) using the high-frequency deflection technique (see Table 3). In contrast, the results from ZB2006 are 165/163 ns, which are significantly lower than the experimental values.

Table 3 compares our calculated lifetimes with other theoretical calculations and experimentally measured results. Other calculation results include B-spline calculation of ZB2006, HFR calculation of Biémont et al. (1998), CI calculation of DH2008, and MCHF calculation of Froese Fischer et al. (2006). In comparison to the others, the HFR results are generally much smaller, except for  $3p3(^2P)4s\ ^3P_{0,1,2}$ ,  $3p^3(^2D)4p\ ^3P_2$ , and  $3p^3(^4S)6d\ ^5D_4^o$ . The theoretical results from the present calculations, as well as those from ZB2006 and DH2008, are in very good agreement with the experimental measurements obtained by Berzinsh et al. (1997) using laser spectroscopy and Beideck et al. (1994) using the beam-foil technique; they are also in good agreement with the astronomical observations by Federman & Cardelli (1995), except for the  $3p^3(^4S)4d\ ^3D_{1,2,3}$  states, where the lifetimes from DH2008 are approximately half of the measured results by Berzinsh et al. (1997). For the long-lived states, namely  $3p^3(^4S)4s\ ^5S_2^o$ ,  $3p^3(^4S)np\ ^5P_3(n = 5, 6, 7)$ , and  $3p^3(^4S)6d\ ^3D_2^o$ , there are significant differences between theoretical and experimental measurements, nor among different calculations and experimental results. For these energy levels, which are dominated by weak transitions, both theoretical calculations and experimental measurements are challenging. In addition, the measurements of lifetimes for long-lived states often have large uncertainties and further precise measurements are needed.

## 4. Conclusion

The energy levels, transition data, and lifetimes of S I were calculated using both the ab initio and fine-tuning approaches based on the MCDHF and RCI methods. We found that fine-tuning provides more accurate mixing coefficients, which correctly position the energy levels. It can also better improve the results in the Coulomb gauge, which is typically less accurate in ab initio calculations. The corrections to the wave functions resulting from fine-tuning improve the consistency of the transition data between the Babushkin and Coulomb gauges, thereby enhancing the accuracy of the transition data.

Table 3: Comparison of experimental and theoretical radiative lifetimes (in units of nanosecond) for S I.

No.	State	Theory						Experiment	
		ab initio B/C	Fine-tuned B/C	B-spline <sup>a</sup> B/C	HFR <sup>b</sup>	CI <sup>c</sup> B/C	MCHF <sup>d</sup>	laboratory measurements	astronomical observations <sup>f</sup>
7	$3p^3(^4S)4s\ ^3S_1$	1.93/1.96	1.94/1.99	1.93/1.98	1.5	1.94/2.05	2.04	1.875(0.094) <sup>g</sup>	1.875(0.188)
27	$3p^3(^4S)5s\ ^3S_1$	6.88/7.01	6.83/6.95	6.87/6.97	4.2	5.92/6.63		7.1(0.5) <sup>e</sup>	6.9(1.4)
54	$3p^3(^4S)6s\ ^3S_1$	16.80/17.20	16.77/17.14	17.0/17.2	9.7	13.72/18.00		17.7(1.1) <sup>e</sup>	16.9(3.4)
90	$3p^3(^4S)7s\ ^3S_1$	34.16/35.38	33.90/35.38	34.5/34.9	18.8			35.6(4.0) <sup>e</sup>	31.0(8.4)
6	$3p^3(^4S)4s\ ^5S_2$	13893/14439	13510/14043	17615/19771		18691/25138	39037	9200(1000) <sup>i</sup> 27000(5000) <sup>j</sup>	
22	$3p^3(^2D)4s\ ^1D_2$	2.23/2.27	2.23/2.27	2.23/2.24	1.7	2.26/2.34	2.30		
55	$3p^3(^2P)4s\ ^3P_0$	2.25/2.29	2.25/2.29	2.22/2.25	3.0	2.29/2.39			
56	$3p^3(^2P)4s\ ^3P_1$	2.24/2.28	2.24/2.28	2.21/2.24	2.9	2.30/2.40		2.034(0.102) <sup>g</sup>	2.1(0.2)
57	$3p^3(^2P)4s\ ^3P_2$	2.22/2.26	2.22/2.26	2.20/2.22	2.8	2.35/2.46		2.146(0.129) <sup>g</sup>	2.1(0.2)
12	$3p^3(^4S)4p\ ^3P_0$	45.12/43.72	45.15/44.80	46.3/45.4	36.1	44.05/43.67	49.5	46.1(1.0) <sup>e</sup>	
11	$3p^3(^4S)4p\ ^3P_1$	45.14/43.74	45.17/44.82	46.3/45.4	36.1	44.04/43.66	49.4	46.1(1.0) <sup>e</sup>	
13	$3p^3(^4S)4p\ ^3P_2$	45.10/43.69	45.12/44.78	46.3/45.4	36.0	44.03/43.65	49.3	46.1(1.0) <sup>e</sup>	
91	$3p^3(^2D)4p\ ^3P_2$	58.49/58.48	58.25/59.46	53.6/53.8	63.0	36.07/32.96		53.5(4) <sup>i</sup>	
34	$3p^3(^4S)5p\ ^3P_2$	179.06/173.11	179.14/178.85	184/186	131.9	141.98/181.15		188(13) <sup>e</sup> 185(15) <sup>i</sup>	
33	$3p^3(^4S)5p\ ^5P_3$	156.05/149.48	155.78/153.94	158/159	130.1	151.49/156.49		615(50) <sup>i</sup>	
60	$3p^3(^4S)6p\ ^5P_3$	352.19/329.68	351.23/346.94	352/350	289.9	481.87/389.08		265(20) <sup>i</sup>	
96	$3p^3(^4S)7p\ ^5P_3$	596.11/621.01	601.79/673.21	631/624	549.8			415(25) <sup>i</sup>	
23	$3p^3(^4S)3d\ ^3D_1$	3.44/3.61	3.52/3.67	3.69/3.77	1.9	4.58/5.11	2.62		
24	$3p^3(^4S)3d\ ^3D_2$	3.44/3.60	3.52/3.66	3.68/3.77	1.9	4.45/4.97	2.61		3.0(0.6)
25	$3p^3(^4S)3d\ ^3D_3$	3.42/3.58	3.50/3.64	3.67/3.75	1.9	4.59/5.16	2.59		
42	$3p^3(^4S)4d\ ^3D_1$	11.87/12.36	11.97/12.48	12.1/12.6	6.0	6.27/7.09		12.6(1.3) <sup>e</sup>	
43	$3p^3(^4S)4d\ ^3D_2$	11.85/12.34	11.96/12.46	12.1/12.6	6.0	6.49/7.43		12.5(0.7) <sup>e</sup>	9.6(1.9)
44	$3p^3(^4S)4d\ ^3D_3$	11.73/12.21	11.84/12.34	12.0/12.5	5.9	6.18/7.02		12.9(1.1) <sup>e</sup>	
80	$3p^3(^4S)5d\ ^3D_1$	37.18/38.84	38.38/39.73	36.0/37.8	10.1			41(3) <sup>e</sup>	
78	$3p^3(^4S)5d\ ^3D_2$	37.68/39.34	38.76/40.09	36.3/38.1	10.0				37(7.5)
79	$3p^3(^4S)5d\ ^3D_3$	37.75/39.39	38.80/40.18	36.6/38.4	9.9			40(4) <sup>e</sup>	
97	$3p^3(^4S)6d\ ^5D_4$	266.27/269.21	264.35/251.99	165/163	593.1			260(20) <sup>i</sup>	
107	$3p^3(^4S)6d\ ^3D_1$	134.65/135.55	141.41/141.03	108/115	16.0				
106	$3p^3(^4S)6d\ ^3D_2$	138.30/139.29	145.68/145.13	112/118	15.9			75(7) <sup>b</sup>	199(90)
105	$3p^3(^4S)6d\ ^3D_3$	142.01/143.06	150.12/149.33	116/123	15.8				

**Notes.** B/C: Babushkin and Coulomb gauges. The values in the parentheses of the last two columns are the experimental errors.

(<sup>a</sup>) B-spline method by [Zatsarinny & Bartschat \(2006\)](#). (<sup>b</sup>) Relativistic Hartree-Fock calculation by [Biémont et al. \(1998\)](#). (<sup>c</sup>) Configuration interaction calculation by [Deb & Hibbert \(2008\)](#). (<sup>d</sup>) Multi-configurational Hartree-Fock calculation by [Froese Fischer et al. \(2006\)](#). (<sup>e</sup>) Laser spectroscopy by [Berzinsh et al. \(1997\)](#) and [Zerne et al. \(1997\)](#). (<sup>f</sup>) Lifetime data excerpted from [Zatsarinny & Bartschat \(2006\)](#) and original from [Federman & Cardelli \(1995\)](#); [Federman & Cardelli \(1996\)](#). (<sup>g</sup>) Beam-foil technique by [Beideck et al. \(1994\)](#). (<sup>i</sup>) High-frequency deflection technique by [Delalic et al. \(1990\)](#). (<sup>j</sup>) Electron-impact dissociation method by [Mason \(1994\)](#).

We conducted extensive comparisons with various theoretical and experimental results. The accuracy level of the computed data was evaluated using a combination of gauge differences parameters and CFs. For applications requiring complete atomic datasets, we recommend using the fine-tuned data in the Babushkin gauge; for specific transitions, cross-validation with different sources is advised to ensure reliability. Notably, significant discrepancies were observed among different theoretical calculations for certain transitions, particularly for the solar-abundance diagnostic lines. The lack of precise experimental measurements complicates the assessment of the accuracy of different calculations. Further experimental efforts are essential to validating and constraining theoretical predictions.

The atomic data provided in this study can be used for astrophysical applications, not least non-LTE stellar spectroscopic analyses (e.g. [Korotin & Kiselev 2024](#)). In particular, the implications of these new data on the solar sulphur abundance were recently discussed in detail in [Amarsi et al. \(2025\)](#).

## Data availability

The full versions of Table A.1 and Table A.2 are only available in electronic form at the CDS via anonymous ftp to [cdsarc.u-strasbg.fr](http://cdsarc.u-strasbg.fr) (130.79.128.5) or via <http://cdsweb.u-strasbg.fr/cgi-bin/qcat?J/A+A/>.

**Acknowledgements.** WL acknowledges the support from the National Key R&D Program of China No. 2022YFF0503800, the National Natural Science Foundation of China (NSFC, Grant No. 12373058) and the specialized research fund for State Key Laboratory of Solar Activity and Space Weather. AMA acknowledges support from the Swedish Research Council (VR 2020-03940) the Crafoord Foundation via the Royal Swedish Academy of Sciences (CR 2024-0015), and the European Union's Horizon Europe research and innovation programme under grant agreement No. 101079231 (EXOHOST). PJ acknowledges support from the Swedish Research Council (VR 2023-05367). AMA and WL also acknowledge support from the 2024 Chinese Academy of Sciences (CAS) President's International Fellowship Initiative (PIFI). WL thanks Yanting Li for the helpful discussion with the rfnetune code. We would also like to thank the anonymous referee for providing useful comments that helped improve the original manuscript.

## References

Amarsi, A. M., Li, W., Grevesse, N., & Jurewicz, A. J. G. 2025, A&A, 703, A35

Anderson, D. E., Bergin, E. A., Maret, S., & Wakelam, V. 2013, The Astrophysical Journal, 779, 141

Beideck, D. J., Schectman, R. M., Federman, S. R., & Ellis, D. G. 1994, ApJ, 428, 393

Berzinsh, U., Caiyan, L., Zerne, R., Svanberg, S., & Biémont, E. 1997, Phys. Rev. A, 55, 1836

Biémont, E., Garnir, H. P., Federman, S. R., Li, Z. S., & Svanberg, S. 1998, ApJ, 502, 1010

Biémont, E., Storey, P. J., & Zeippen, C. J. 1996, A&A, 309, 991

Bridges, J. M. & Wiese, W. L. 1967, Physical Review, 159, 31

Caffau, E., Faraggiana, R., Bonifacio, P., Ludwig, H.-G., & Steffen, M. 2007, A&A, 470, 699

Carpenter, K. G., Robinson, R. D., Wahlgren, G. M., Linsky, J. L., & Brown, A. 1994, ApJ, 428, 329

Chen, M. H., Cheng, K. T., & Johnson, W. R. 2001, Phys. Rev. A, 64, 042507

Chen, Z. & Msezane, A. Z. 1997, Journal of Physics B Atomic Molecular Physics, 30, 3873

Civiš, S., Kramida, A., Zanoina, E. M., et al. 2024, ApJS, 274, 32

Corrége, G. & Hibbert, A. 2004, Atomic Data and Nuclear Data Tables, 86, 19

Costa Silva, A. R., Delgado Mena, E., & Tsantaki, M. 2020, A&A, 634, A136

Cowan, R. D. 1981, The Theory of Atomic Structure and Spectra, 1st edn., Vol. 3 (University of California Press)

da Silva, R., D’Orazi, V., Palla, M., et al. 2023, A&A, 678, A195

Daflon, S., Cunha, K., Smith, V. V., & Butler, K. 2003, A&A, 399, 525

Deb, N. C. & Hibbert, A. 2006, Journal of Physics B Atomic Molecular Physics, 39, 4301

Deb, N. C. & Hibbert, A. 2008, Atomic Data and Nuclear Data Tables, 94, 561

Delalic, Z., Erman, P., & Kallne, E. 1990, Phys. Scr, 42, 540

Doering, J. P. 1990, J. Geophys. Res., 95, 21313

Duffau, S., Caffau, E., Sbordone, L., et al. 2017, A&A, 604, A128

Durrance, S. T., Feldman, P. D., & Weaver, H. A. 1983, ApJ, 267, L125

Dyall, K., Grant, I., Johnson, C., Parpia, F., & Plummer, E. 1989, Comput. Phys. Commun., 55, 425

Ekman, J., Godefroid, M., & Hartman, H. 2014, Atoms, 2, 215

Fawcett, B. C. 1986, Atomic Data and Nuclear Data Tables, 35, 185

Feaga, L. M., McGrath, M. A., & Feldman, P. D. 2002, ApJ, 570, 439

Federman, S. R. & Cardelli, J. A. 1995, ApJ, 452, 269

Federman, S. R. & Cardelli, J. A. 1996, Physica Scripta, 1996, 158

Fischer, C. F. 1987, Journal of Physics B: Atomic and Molecular Physics, 20, 4365

Fleming, J. & Hibbert, A. 1999, Physica Scripta Volume T, 83, 44

Froese Fischer, C. 2009, Physica Scripta Volume T, 134, 014019

Froese Fischer, C., Gaigalas, G., Jönsson, P., & Bieroń, J. 2019, Comput. Phys. Commun., 237, 184

Froese Fischer, C., Godefroid, M., Brage, T., Jönsson, P., & Gaigalas, G. 2016, Journal of Physics B: Atomic, Molecular and Optical Physics, 49, 182004

Froese Fischer, C. & Tachiev, G. 2004, Atomic Data and Nuclear Data Tables, 87, 1

Froese Fischer, C., Tachiev, G., Gaigalas, G., & Godefroid, M. R. 2007, Computer Physics Communications, 176, 559

Froese Fischer, C., Tachiev, G., & Irimia, A. 2006, Atomic Data and Nuclear Data Tables, 92, 607

Gaigalas, G., Fritzsche, S., & Grant, I. P. 2001, Computer Physics Communications, 139, 263

Gaigalas, G., Froese Fischer, C., Rynkun, P., & Jönsson, P. 2017, Atoms, 5, 6

Gaigalas, G., Rudzikas, Z., & Froese Fischer, C. 1997, Journal of Physics B Atomic Molecular Physics, 30, 3747

Gaigalas, G., Rynkun, P., Domoto, N., et al. 2024, MNRAS, 530, 5220

Gaigalas, G., Rynkun, P., Radžiūtė, L., et al. 2020, ApJS, 248, 13

Gaigalas, G., Žalandauskas, T., & Rudzikas, Z. 2003, Atomic Data and Nuclear Data Tables, 84, 99

Gaigalas, G., Žalandauskas, T., & Fritzsche, S. 2004, Computer Physics Communications, 157, 239

Ganas, P. S. 1982, Physics Letters A, 87, 394

Grant, I. P. 1974, Journal of Physics B Atomic Molecular Physics, 7, 1458

Grant, I. P. 2007, Relativistic Quantum Theory of Atoms and Molecules (Springer, New York)

Hibbert, A. 1974, Journal of Physics B: Atomic and Molecular Physics, 7, 1417

Hibbert, A. 1975, Computer Physics Communications, 9, 141

Ho, Y. K. & Henry, R. J. W. 1985, ApJ, 290, 424

Judge, P. G. 1988, MNRAS, 231, 419

Jönsson, P., Gaigalas, G., Fischer, C. F., et al. 2023a, Atoms, 11

Jönsson, P., Godefroid, M., Gaigalas, G., et al. 2023b, Atoms, 11

Kamp, I., Iliev, I. K., Paunzen, E., et al. 2001, A&A, 375, 899

Kaufman, V. & Martin, W. C. 1993, Journal of Physical and Chemical Reference Data, 22, 279

Korotin, S. A. & Kiselev, K. O. 2024, Astronomy Reports, 68, 1159

Kramida, A., Yu. Ralchenko, Reader, J., & and NIST ASD Team. 2024, NIST Atomic Spectra Database (ver. 5.12), [Online]. Available: <https://physics.nist.gov/asd> [2025, August 21]. National Institute of Standards and Technology, Gaithersburg, MD.

Kurucz, R. L. & Peytremann, E. 1975, SAO Special Report

Laverick, M., Lobel, A., Royer, P., et al. 2019, A&A, 624, A60

Li, M. C., Li, W., Jönsson, P., Amarsi, A. M., & Grumer, J. 2023a, ApJS, 265, 26

Li, W., Jönsson, P., Amarsi, A. M., Li, M. C., & Grumer, J. 2023b, A&A, 674, A54

Li, Y., Gaigalas, G., Li, W., Chen, C., & Jönsson, P. 2023, Atoms, 11

Lundberg, H., Li, Z. S., & Jönsson, P. 2001, Phys. Rev. A, 63, 032505

Mason, N. J. 1994, Physica Scripta, 49, 578

Müller, D. 1968, Zeitschrift Naturforschung Teil A, 23, 1707

Nissen, P. E., Akerman, C., Asplund, M., et al. 2007, A&A, 469, 319

Olsen, J., Roos, B. O., Jørgensen, P., & Jensen, H. J. A. 1988, The Journal of chemical physics, 89, 2185

Papouli, A., Ekman, J., Gaigalas, G., et al. 2019, Atoms, 7

Papouli, A., Ekman, J., & Jönsson, P. 2019, A&A, 621, A16

Podobedova, L. I., Kelleher, D. E., & Wiese, W. L. 2009, Journal of Physical and Chemical Reference Data, 38, 171

Savage, B. D. & Lawrence, G. M. 1966, ApJ, 146, 940

Scott, P., Grevesse, N., Asplund, M., et al. 2015, A&A, 573, A25

Skillman, E. D. & Kennicutt, Jr., R. C. 1993, ApJ, 411, 655

Skúladóttir, Á., Andrievsky, S. M., Tolstoy, E., et al. 2015, A&A, 580, A129

Starace, A. F. 1971, Phys. Rev. A, 3, 1242

Sturesson, L., Jönsson, P., & Froese Fischer, C. 2007, Computer physics communications, 177, 539

Takeda, Y., Hashimoto, O., Taguchi, H., et al. 2005, PASJ, 57, 751

Tayal, S. S. 1998, ApJ, 497, 493

Tennyson, J. 2019, Astronomical Spectroscopy. An Introduction to the Atomic and Molecular Physics of Astronomical Spectroscopy (World Scientific)

Zatsarinny, O. & Bartschat, K. 2006, Journal of Physics B Atomic Molecular Physics, 39, 2861

Zerne, R., Caiyan, L., Berzinsh, U., & Svanberg, S. 1997, Physica Scripta, 56, 459

Zhang, W., Palmeri, P., Quinet, P., & Biémont, É. 2013, A&A, 551, A136

## Appendix A: Energy levels and transition data.

Table A.1: Energy levels and lifetimes from ab initio and fine-tuning calculations.

No.	Configuration	State	E (cm <sup>-1</sup> )			ab initio		Fine-tuned	
			ab initio	fine-tuned	NIST ASD	$\tau_B$ (s)	$\tau_C$ (s)	$\tau_B$ (s)	$\tau_C$ (s)
1	3p <sup>4</sup>	<sup>3</sup> P <sub>2</sub>	0.00	0.00	0.0000				
2	3p <sup>4</sup>	<sup>3</sup> P <sub>1</sub>	388.63	395.37	396.0565				
3	3p <sup>4</sup>	<sup>3</sup> P <sub>0</sub>	563.86	572.33	573.5957				
4	3p <sup>4</sup>	<sup>1</sup> D <sub>2</sub>	9423.71	9258.76	9238.6090				
5	3p <sup>4</sup>	<sup>1</sup> S <sub>0</sub>	22798.74	22276.12	22179.9542				
6	3p <sup>3</sup> ( <sup>4</sup> S)4s	<sup>5</sup> S <sub>2</sub> <sup>0</sup>	52206.08	52586.28	52623.6050	1.389E-05	1.444E-05	1.351E-05	1.404E-05
7	3p <sup>3</sup> ( <sup>4</sup> S)4s	<sup>3</sup> S <sub>1</sub> <sup>0</sup>	54980.58	55302.32	55330.7750	1.931E-09	1.964E-09	1.944E-09	1.985E-09
8	3p <sup>3</sup> ( <sup>4</sup> S)4p	<sup>5</sup> P <sub>1</sub>	62952.47	63405.52	63446.0380	3.605E-08	3.567E-08	3.616E-08	3.606E-08
9	3p <sup>3</sup> ( <sup>4</sup> S)4p	<sup>5</sup> P <sub>2</sub>	62963.20	63416.88	63457.1166	3.595E-08	3.558E-08	3.606E-08	3.596E-08
10	3p <sup>3</sup> ( <sup>4</sup> S)4p	<sup>5</sup> P <sub>3</sub>	62980.48	63434.97	63475.0270	3.577E-08	3.540E-08	3.588E-08	3.579E-08
—	—	—	—	—	—	—	—	—	—

**Notes.** Energy levels are given relative to the ground state and are compared with the NIST ASD data (Kramida et al. 2024) that originates from Civiš et al. (2024). The lifetimes are given in Babushkin ( $\tau_B$ ) and Coulomb ( $\tau_C$ ) gauges, respectively. The excitation energies for No. 94 and 95 are not available in the NIST ASD. Considering the close degeneracies in these states, we used the energy value of No. 96 (3p<sup>3</sup>(<sup>4</sup>S)7p <sup>5</sup>P<sub>3</sub>) as the energies for No. 94 and 95 in the fine-tuning procedure. Full table is available at the CDS.

Table A.2: Computed transition data.

Upper state	Lower state	$\lambda$ (Å)	ab initio						fine-tuned					
			log(gf)		A (s <sup>-1</sup> )		Acc		log(gf)		A (s <sup>-1</sup> )		Acc.	
			B	C	B	C	B	C	B	C	B	C	B	C
3p <sup>3</sup> ( <sup>4</sup> S)6d <sup>3</sup> D <sub>1</sub> <sup>0</sup>	3p <sup>4</sup> <sup>3</sup> P <sub>2</sub>	1247.11	-4.01	-3.98	1.39E+05	1.50E+05	C	C	-4.04	-4.01	1.29E+05	1.39E+05	C	C
3p <sup>3</sup> ( <sup>4</sup> S)6d <sup>3</sup> D <sub>2</sub> <sup>0</sup>	3p <sup>4</sup> <sup>3</sup> P <sub>2</sub>	1247.14	-2.86	-2.83	1.17E+06	1.26E+06	C	C	-2.90	-2.87	1.08E+06	1.17E+06	C	C
3p <sup>3</sup> ( <sup>4</sup> S)6d <sup>3</sup> D <sub>3</sub> <sup>0</sup>	3p <sup>4</sup> <sup>3</sup> P <sub>2</sub>	1247.16	-2.15	-2.12	4.32E+06	4.67E+06	C	C	-2.19	-2.16	3.93E+06	4.27E+06	C	C
3p <sup>3</sup> ( <sup>4</sup> S)6d <sup>5</sup> D <sub>3</sub> <sup>0</sup>	3p <sup>4</sup> <sup>3</sup> P <sub>2</sub>	1250.12	-6.43	-7.27	2.28E+02	3.25E+01	E	E	-5.82	-6.13	9.14E+02	4.54E+02	E	E
3p <sup>3</sup> ( <sup>4</sup> S)6d <sup>5</sup> D <sub>3</sub> <sup>0</sup>	3p <sup>4</sup> <sup>3</sup> P <sub>2</sub>	1250.12	-6.13	-6.43	6.37E+02	3.20E+02	E	E	-6.14	-6.45	6.20E+02	3.04E+02	E	E
3p <sup>3</sup> ( <sup>4</sup> S)6d <sup>5</sup> D <sub>5</sub> <sup>0</sup>	3p <sup>4</sup> <sup>3</sup> P <sub>2</sub>	1250.12	-6.50	-6.71	4.50E+02	2.79E+02	E	E	-6.56	-6.79	3.89E+02	2.28E+02	E	E
3p <sup>3</sup> ( <sup>4</sup> S)6d <sup>3</sup> D <sub>1</sub> <sup>0</sup>	3p <sup>4</sup> <sup>3</sup> P <sub>1</sub>	1253.30	-2.85	-2.82	1.99E+06	2.14E+06	C	C	-2.89	-2.86	1.84E+06	1.97E+06	C	C
3p <sup>3</sup> ( <sup>4</sup> S)6d <sup>3</sup> D <sub>2</sub> <sup>0</sup>	3p <sup>4</sup> <sup>3</sup> P <sub>1</sub>	1253.33	-2.40	-2.37	3.35E+06	3.60E+06	C	C	-2.44	-2.41	3.07E+06	3.30E+06	C	C
3p <sup>3</sup> ( <sup>4</sup> S)6d <sup>5</sup> D <sub>2</sub> <sup>0</sup>	3p <sup>4</sup> <sup>3</sup> P <sub>1</sub>	1256.34	-8.91	-7.70	1.04E+00	1.67E+01	E	E	-8.56	-7.86	2.31E+00	1.16E+01	E	E
3p <sup>3</sup> ( <sup>4</sup> S)6d <sup>3</sup> D <sub>1</sub> <sup>0</sup>	3p <sup>4</sup> <sup>3</sup> P <sub>1</sub>	1256.34	-6.48	-6.76	4.68E+02	2.44E+02	E	E	-6.66	-7.03	3.04E+02	1.31E+02	E	E
—	—	—	—	—	—	—	—	—	—	—	—	—	—	—

**Notes.** Only the first ten rows are shown. The wavelengths are vacuum wavelengths obtained based on the energy levels in the NIST ASD originated from Civiš et al. (2024). It should be noted that the wavelengths of the transitions associated with No. 94 and 95 (3p<sup>3</sup>(<sup>4</sup>S)7p <sup>5</sup>P<sub>1,2</sub>) were calculated using the energy value of No. 96 (3p<sup>3</sup>(<sup>4</sup>S)7p <sup>5</sup>P<sub>3</sub>). Full table is available at the CDS.